2021

Suitable low Global Warming Potential (GWP) refrigerants for two-speed Heat Pumps for residential applications based on simulated performance

Shen Bo
Oak Ridge National Laboratory

Moonis Ally
allymr@ornl.gov

Sharma Vishaldeep

Suitable low Global Warming Potential (GWP) refrigerants for cold climate heat pumps (CCHPs) for residential applications based on simulated performance

Bo SHEN[1], Moonis R. ALLY[1]*, Vishaldeep SHARMA[1]

[1]Energy and Transportation Sciences Division, Oak Ridge National Laboratory[1],
Oak Ridge, TN, USA
Contact Information (Phone, 865-576-8003, Fax, 865-574-9338, allymr@ornl.gov)

* Corresponding Author

ABSTRACT

The next generation of heat pumps (HPs), including those intended for cold climates must transition to low- global warming potential (GWP) refrigerants to mitigate climate change. HPs must be designed to alleviate the problems of excessive discharge temperatures, low suction pressure and high-pressure ratio at low ambient conditions and insufficient heating capacity relative to the rated heating capacity. In this paper we recognize those concerns. Low global warming potential (GWP) refrigerants are screened based on the shape of their temperature-entropy (T-S) saturation boundary. Simulations of the two-stage HP with low GWP refrigerants (R32, R454B, R466A, and R452B) to replace R-410A was accomplished using the DOE/ORNL Heat Pump Design Model. Systemic inefficiency was addressed by component-level exergy analysis to refine design options. HPs with low-GWP refrigerants address issues of reducing energy consumption, lowering carbon footprint, and enabling environmental sustainability.

1. INTRODUCTION

To replace HCFC and HFC refrigerants in existing air conditioner/heat pump equipment, selections of alternative lower GWP refrigerants are subject to a few key factors. The candidates should possess similar volumetric capacity so that available compressors would provide similar cooling capacity and equal or higher energy efficiency. They should accommodate the same or wider working envelope, i.e. an adequately high refrigerant critical temperature for high ambient cooling operation. Compressor discharge temperature should be limited to prevent the need to change compressor lubricant and maintain good reliability. Refrigerants should not have a re-entrant region to avoid "wet-compression" leading to premature compressor degradation (Morrison, 1994; Ally et al., 2019).

Potential low GWP replacement refrigerants for R-410A are shown in Table 1. Mostly these are either R-32 or blends containing R-32 and an HFO (Hydrofluoroolefins, e.g., R-1234yf). They have approximately 70% lower GWPs than R-410A. On the other hand, three of the candidates are classified as A2L or mildly flammable. It should be noted that R-466A is an A1 refrigerant, i.e. non-flammable. These refrigerant blends have negligible temperature glides. All the alternatives have higher critical temperatures than R-410A, making them more suitable for high condensing temperature operation.

Table 1: Alternative Low GWP Replacements for R-410A

Refrigerant	GWP AR4[a]	GWP AR5[b]	Safety Class	Temperature glide [K]	Critical T [C]
R-410A[c]	2088	1924	A1	0.1	71.34
R-32	675	677	A2L	0.0	78.12
R-452B[d]	698	676	A2L	1.3	79.68
R-454B[e]	466	467	A2L	1.5	77.0
R-466A[f]	733	733	A1	1.5	83.8

[a]IPCC 2007.; [b]IPCC 2013.; [c]R-410A has mass-based compositions of R-32 (0.5)/R-125 (0.5).; [d]R-452B has mass-based compositions of R-32 (0.67)/R-125 (0.07)/R-1234yf (0.26).; [e]R-454B has mass-based compositions of R-32 (0.689)/R-1234yf (0.311).; [f]R-466A has mass-based compositions of R-32 (0.49) / R-125 (0.115) / R-13I (0.395).

2. REFRIGERANT PROPERTIES

The temperature-enthalpy diagram of a refrigerant illustrates two critical properties: the span between the saturated liquid line and saturated vapor line (i.e. latent heat of vaporization per unit mass of refrigerant) and the critical temperature (working range). Volumetric heat of vaporization, i.e. latent heat × vapor density at an average saturation temperature of dew point and bubble point, indicates the evaporating capacity per unit volumetric flow rate. Refrigerants with smaller volumetric vaporization heat have reduced cooling capacities at a fixed compressor displacement volume.

Figure 1 illustrates the temperature-enthalpy diagrams of R-410A and the alternative refrigerants in Table 1. All the alternatives (except R-466A) have wider domes and higher critical temperatures than R-410A, indicating that they are better refrigerants for high ambient operations. Figure 2 shows the volumetric vaporization heat versus the average saturation temperature. R-32 has noticeably larger vaporization heat than R-410A, and R-466A is slightly larger. R-452B and R-454B have similar vaporization heat, which are slightly lower than R-410A. Figure 3 shows curves of saturation temperature versus density of the R-410A alternatives. Most of the R-410A alternatives, except R-466A, have lower suction vapor density and consequently smaller refrigerant mass flow rate for a fixed compressor displacement volume. At an average saturation temperature, a refrigerant with a lower volumetric heat of vaporization results in smaller cooling capacity for a drop-in replacement. The saturation temperature is also impacted by the heat transfer performance and refrigerant pressure drop of the refrigerant. Lower saturation temperature leads to smaller cooling capacity if using the same compressor. And thus, whether an alternative low GWP refrigerant leads to higher or lower capacity depends on the trade-off between its volumetric vaporization heat and the resultant suction saturation temperature impacted by its heat transfer characteristics.

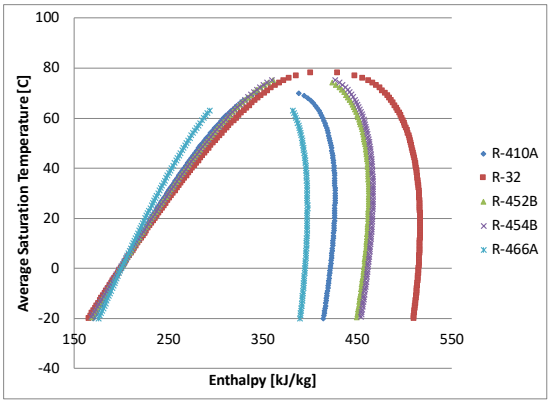

Figure 1: Temperature-enthalpy plots of R-410A alternatives.

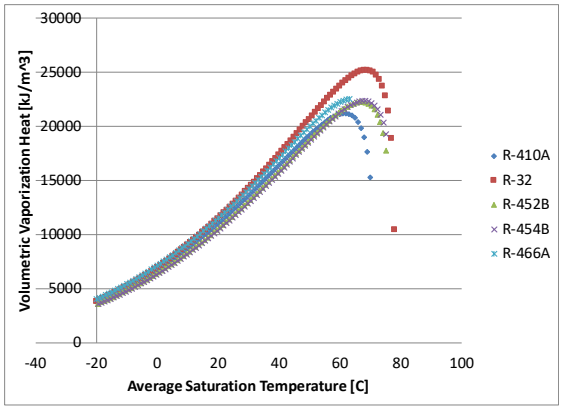

Figure 2: Volumetric vaporization heat plot of R-410A alternatives.

In a typical vapor compression cycle, the phenomenon of "wet compression" occurs with the formation of liquid during compression with refrigerants that exhibit skewness in the temperature-entropy (T-S) saturation phase boundary (**Figure 4**). The degree of skewness of the saturation boundary characterizes the severity of the re-entrant region. A re-entrant region occurs when the vertical vapor phase line crosses the T-S curve at three discrete points due to skewness (Morrison, 1994; Ally et al., 2019). The formation of a liquid phase during compression can cause extensive mechanical damage to a compressor, and lower efficiency during seemingly normal use (*ibid.*). For the alternative refrigerants, we see no evidence of any re-entrant behaviour as shown in **Figure 4**.

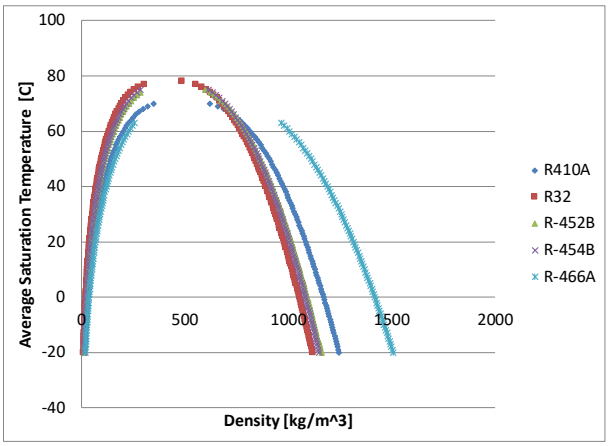

Figure 3: Saturation temperature-density curves

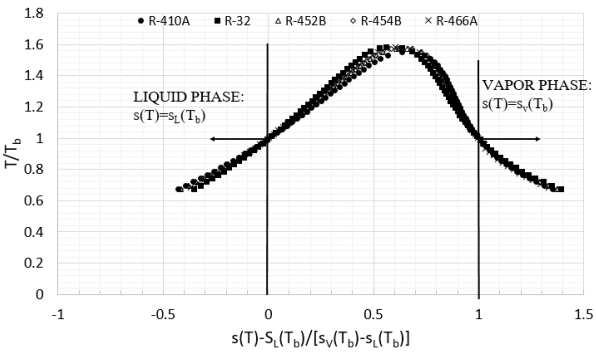

Figure 4: T-S diagrams for R-410A and alternatives show no skewness, implying no re-entrant region.

3. MODEL DESCRIPTION

The DOE/ORNL Heat Pump Design Model (HPDM (Shen and Rice, 2016) was used to model a baseline heat pump. HPDM is a well-known, public-domain HVAC equipment modelling and design tool. It has a free web interface and downloadable desktop version to support public use. Some features of the HPDM, related to this study, are introduced below:

Compressor model: AHRI 10-coefficient compressor maps (ANSI/AHRI 540-99, 2010) are used to calculate mass flow rate and power consumption, and enable calculation of the refrigerant-side vs. air-side energy balance from inlet to outlet by inputting a compressor shell loss ratio relative to the power input. It also considers the actual suction state to correct the map mass flow prediction using the method of Dabiri and Rice (1981). We obtained the original compressor maps, developed for R-410A. For modeling the alternative refrigerants, it was assumed that the compressor would maintain the same volumetric and isentropic efficiencies for all the refrigerants studied at the same suction and discharge pressures. Thus, the efficiencies were defined from the original R-410A map using Eq.s 1 and 2.

$$m_r = Volume_{displacement} \times Speed_{rotation} \times Density_{suction} \times \eta_{vol} \quad (1)$$

$$Power = m_r \times \frac{\left(H_{discharge,s} - H_{suction}\right)}{\eta_{isentropic}} \quad (2)$$

Where $\boldsymbol{m_r}$ is compressor mass flow rate; $\boldsymbol{Power}$ is compressor power; $\boldsymbol{\eta_{vol}}$ is compressor volumetric efficiency; $\boldsymbol{\eta_{isentropic}}$ is compressor isentropic efficiency; $\boldsymbol{H_{suction}}$ is compressor suction enthalpy; $\boldsymbol{H_{discharge,s}}$ is the enthalpy obtained at the compressor discharge pressure and suction entropy. The approach converting the compressor map of a baseline refrigerant to be used by its drop-in replacements has been extensively validated in Shen *et al.* (2018).

Heat Exchanger Models:

Segment-to-segment fin-&-tube condenser: It uses a segment-to-segment modelling approach, which divides a single tube to numerous mini segments; each tube segment has individual air side and refrigerant side entering states and considers possible phase transition. An ε-NTU approach is used for heat transfer calculations within each segment.

Air-side fin is simplified as an equivalent annular fin. Both refrigerant and air-side heat transfer and pressure drop are considered. The coil model can simulate arbitrary tube and fin geometries and circuitries, any refrigerant side entering and exit states, maldistribution, and accept two-dimensional air side temperature, humidity and velocity local inputs; the tube circuitry and 2-D boundary conditions are provided by an input file.

Segment-to-segment fin-&-tube evaporator: In addition to the functionalities of the segment-to-segment fin-tube condenser, the evaporator model is capable of simulating dehumidification process. The method of Braun *et al*., (1989) is used to simulate cases of water condensing on an evaporating coil, where the driving potential for heat and mass transfer is the difference between enthalpies of the inlet air and saturated air at the refrigerant temperature. As noted, the segment-to-segment modelling approach can reveal the glide of a zeotropic refrigerant, since the temperature increment is accounted by each individual segment along the refrigerant flow path.

Through an extensive literature survey, we identified heat transfer and pressure drop correlations suitable for modeling and optimizing air conditioners and heat pumps, to assess various low GWP refrigerants. The correlations are listed in Table 2.

Table 2: Selected correlations for two-phase heat transfer and pressure drop.

Application	Correlation
Fin-&-tube heat exchanger (FTC) -Evaporation heat transfer	Thome and Ei Hajal (2002)
FTC-Condensation heat transfer	Cavallini et al. (2006)
FTC-Evaporation pressure drop	Kedzierski and Choi (1999)
FTC-Condensation pressure drop	Kedzierski and Choi (1999)

The two-phase heat transfer correlations developed by Thome and Ei Hajal (2002) and Cavallini *et al.,* (2006) account for local flow patterns, considering refrigerant properties. The idea of the flow-pattern dependent evaporation model is to first estimate the wetted surface inside a horizontal smooth tube using a flow map prediction. The model covers stratified flow, stratified-wavy, annular-wavy, intermittent, annular flow, annular flow with partial dry-out, and mist flow in evaporation. The general expression for local evaporating heat transfer coefficient is of the form,

$$h_{tp} = \frac{\theta_{dry} h_v + (2\pi - \theta_{dry}) h_{wet}}{2\pi} \tag{3}$$

$$h_{wet} = (h_{nb}^3 + h_{cb}^3)^{1/3} \tag{4}$$

In Eq. (3), θ_{dry} is the dry angle corresponding to the dry circumference of the tube, which is determined from the flow pattern and void fraction. The void fraction model for this correlation is Rouhani and Axelsson (1970). h_{wet} in Eq. (4) is the heat transfer coefficient at the wet circumference of the tube, which is composed of a nucleate boiling term h_{nb} and a convective boiling term h_{cb}. h_v is the heat transfer coefficient at the dry circumference of the tube.

The local evaporation heat transfer coefficient calculated with the Thome and Ei Hajal (2002) correlation is shown in **Figure 5**. The Thome and Ei Hajal (2002) correlation reasonably predicts degradation of heat transfer coefficient at high quality due to dry out of the liquid film, while most of the other correlations are not able to do this. This model can also reveal the effect of heat flux.

The condensation correlation of Cavallini *et al.,* (2006) is given in Eq. 5,

$$h_{tp} = \frac{\theta_{film} h_f + (2\pi - \theta_{film}) h_c}{2\pi} \tag{5}$$

where, θ_{film} is the falling film angle around the perimeter of the tube, which is dependent on the local flow pattern and void fraction. h_f is the Nusselt film condensing coefficient, and h_c is the convective condensation heat transfer coefficient. The Cavallini *et al.,* (2006) condensation model also starts with the flow pattern prediction.

It is reported that azeotropic refrigerant mixtures have the same heat transfer performance as pure refrigerants. Thus, pure refrigerant correlations can work for an azeotropic refrigerant mixture such as R-410A. However, zeotropic refrigerant mixtures with large temperature glides, have different behaviors.

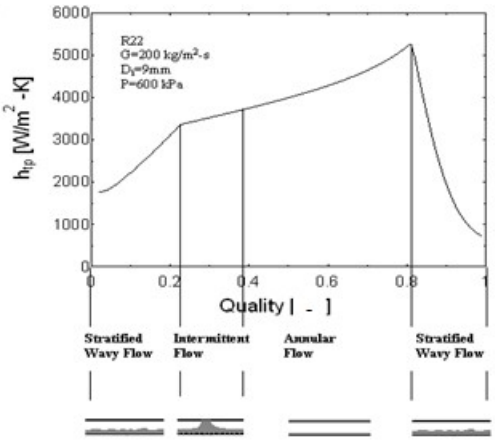

Figure 5: Local flow boiling coefficient predicted with the Thome and Ei Hajal (2002) flow-pattern-dependent evaporation model.

Heat transfer correlations developed for pure refrigerants must be corrected if they are to be used for zeotropic refrigerants. Stephan (1992) proposed a correction method for condensation as well as evaporation. In this method, the mixture heat transfer coefficient h_m is defined as,

$$h_m = \left[1/h_f + \left(\frac{\delta Q_{SV}}{\delta Q_T}\right)/h_g\right]^{-1} \tag{8}$$

where h_f is the heat transfer coefficient computed from a pure refrigerant heat transfer model and h_g is the heat transfer coefficient of the vapor phase, which can be calculated with the Dittus-Boelter equation. $\delta Q_{SV}/\delta Q_T$ is the ratio between the sensible heat transfer and the total heat transfer. Bell (1973) suggested that if the total isobaric temperature glide is around 7-8 °C, then the ratio could be approximated by,

$$\delta Q_{SV}/\delta Q_T \approx x C_{p_g}(\Delta T/\Delta h_m) \tag{7}$$

Where ΔT is the temperature glide, Δh_m is the enthalpy of latent heat of the mixture, x is the quality, and Cp_g is the specific heat of the vapor. We adopted air side heat transfer correlations specific to individual fin types, respectively for dry and wet surfaces.

Expansion Devices: The compressor suction superheat degree and condenser subcooling degree or system charge are explicitly specified. As such, the expansion device is not solved here – a simple assumption of constant enthalpy process is assumed.
Fans and Blowers: The air flow rate and power consumption were direct inputs from the laboratory measurements for the model calibrations.
Refrigerant Lines: Temperature changes and pressure drops of suction, discharge and liquid lines were specified using the measured data from the experiments.
Refrigerant Properties: We programmed interface functions to call REFPROP 10.0 (Lemmon, 2010) [5] directly; our models accept all the refrigerant types in the REFPROP 10.0 database, and also we can simulate a new refrigerant by making the refrigerant definition file according to the REFPROP 10.0 format, or look-up tables.

3. BASELINE HEAT PUMP AND RATING CONDITIONS

The DOE/ORNL heat pump design model (HPDM) was used for analytical evaluations for a baseline heat pump having a two-speed compressor. The two-stage heat pump has a total cooling capacity of 5-ton/17.6 kW at 35°C ambient temperature/26.7°C indoor dry bulb temperature (DB) and 19.4°C indoor wet bulb temperature (WB). The high and low speeds of the scroll compressor provide 100%/67% capacity. The indoor and outdoor heat exchangers are described in Table 3. For the system modeling, the condenser exit subcooling degree was set at 10 R (5.6 K) for cooling mode and 20 R (11.2 K) for heating mode; the evaporator exit was assumed to have a constant superheat degree of 10 R (5.6 K).

Table 3 Parameters of Indoor and Outdoor Units

Parameters (heating mode)	Indoor Fin-&-Tube Coil	Outdoor Fin-&-Tube Coil
Face area, ft2 (m^2)	3.30 (0.307)	22.3 (2.07)
Total Tube Number	84	64
Number of rows	3 (cross counter-flow)	2 (cross counter-flow)
Number of parallel circuits	9	6
Fin density, fins/ft (fins/m)	168 (551)	264 (866)
	Indoor Blower[1] (High/Low)	Outdoor Fan
Flow Rate, cfm (m^3/s)	1670/1380 (0.790/0.653)	3500 (1.652)
Power [W]	322/203	300

[1] The indoor blower has two speed levels, corresponding to the compressor low/high speeds respectively.

Standard AHRI 210/240 (AHRI 2008) rating conditions were used. In cooling mode, 35°C, 27.8°C ambient temperature conditions and 26.7°C DB/19.4°C WB indoor conditions. In heating mode, a single indoor dry bulb temperature condition of 21.1°C is specified. At the low speed, the ambient temperature should vary at 16.7°C DB/13.6°C WB, 8.3°C DB/ 6.1°C WB, 1.7°C DB / 0.6°C WB and -8.3°C DB / -9.4°C WB. The high speed should be rated at 8.3°C DB/ 6.1°C WB, 1.7°C DB / 0.6°C WB and -8.3°C DB / -9.4°C WB.

Since HPDM is a steady-state system model, it doesn't predict cyclic performance and frost/defrost penalty. We adopted a typical degradation coefficient of 0.1 for the high speed, and 0.15 for the low speed. AHRI 210/240 quantifies frosting/defrost loss at the outdoor condition of 1.7°C DB / 0.6°C WB. If no frost effect is correlated by an analytical model, the standard recommends a 98% factor to scale the power consumption and a 91% factor to scale the heating capacity. AHRI 210/240 assumes no frost formation at the ambient temperature above 8.3°C DB/ 6.1°C WB and below -8.3°C DB / -9.4°C WB. At other ambient conditions, the performances are interpolated between 8.3°C DB/ 6.1°C WB, 1.7°C DB / 0.6°C WB; and interpolated between 1.7°C DB / 0.6°C WB and -8.3°C DB / -9.4°C WB. For the ambient conditions below -8.3°C DB / -9.4°C WB, the results are extrapolated based on the predicted results at 8.3°C DB/ 6.1°C WB and -8.3°C DB / -9.4°C WB.

4. COOLING PERFORMANCE

Table 4 below presents predicted cooling performances of the heat pump using R-410A at the low (_L) and high speed (_H) levels, including cooling capacities [kW], cooling COPs [W/W], compressor discharge temperature [C/F] and compressor isentropic efficiency from the compressor map in the form of Eq. 2. The two-speed scroll compressor uses the full displacement volume at 100% capacity. At 67% capacity, only part of the scroll is utilized, which causes more loss factors. As a result, the compressor efficiency of the low speed is roughly 7% lower than the high speed.

Table 4: Parameters of indoor and outdoor units

Outdoor Condition	Capacity [kW]	COP [W/W]	Compressor Disc T [C/F]	Isentropic efficiency
35C_H	17.6	3.7	73.38/164.1	74%
27.7C_H	18.7	4.5	64.11/147.4	73%
35C_L	13.0	3.9	70.38/158.7	67%

27.7C_L	13.9	4.8	60.23/140.5	67%

Figure 6 shows cooling capacity increments of the alterative refrigerants in comparison to R-410A when dropped into the same equipment. Corresponding to the vaporization plots in **Figure 2**, R-32 and R-466A result in 4% to 6% higher cooling capacities at all the conditions. On the other hand, R-452B and R-454B lead to approximately 2% smaller capacities. **Figure 7** shows COP increments. With the same heat exchangers, larger capacity tends to cause higher condensing temperature and lower evaporating temperature, degrading the efficiency. Consequently, R-32 and R-466A have large capacities at the expense of reduced COPs. R-452B and R-454B result in higher COPs**. Figure 8** presents compressor discharge temperatures. R-32 has significantly higher discharge temperatures, up to 30R, while the other alternative refrigerants show lesser increases, up to10R. At the low speed, the discharge temperatures are lower than those at the high speed, because the condensing temperature is reduced at the part-load operation. **Figure 9** compares the seasonal cooling COPs, calculated from AHRI 210/240. Differences relative to R-4110A are minor, ranging from 4.45 to 4.58. R-454B results in the highest COP and R-466A results in the lowest COP.

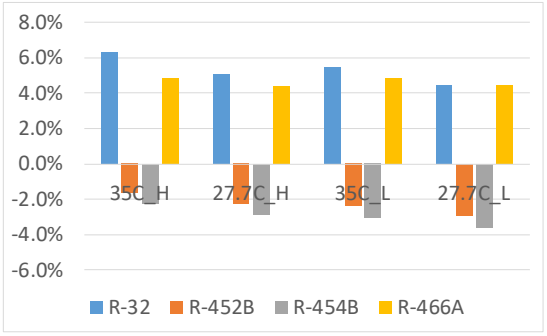

Figure 6: Capacity increments in cooling mode

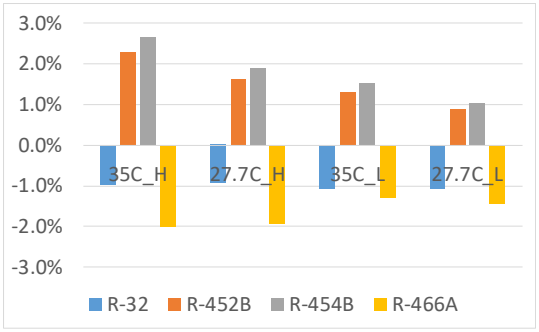

Figure 7: COP increments in cooling mode

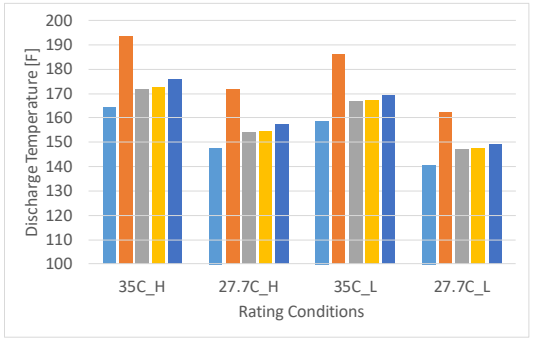

Figure 8: Compressor discharge temperatures (cooling mode)

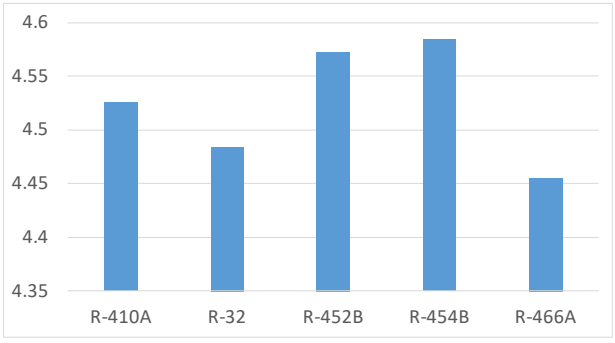

Figure 9: Seasonal cooling COPs

4.1 Exergy Analysis (Cooling)

The method for calculating the exergy losses is developed from applying the First, (**Eq. (8)**) and Second (**Eq. (9)**) Laws of thermodynamics to the steady-steady-flow process in the heat pump cycle.

$$\sum Q_{cv} + W_{cv} + \sum_{in} m_r \left(h + {v^2}/{2} + gz\right) - \sum_{0ut} m_r \left(h + {v^2}/{2} + gz\right) = \frac{dE_{cv}}{dt} = 0 \quad (8)$$

$$\frac{ds_{cv}}{dt} = 0 = \sum_{out} m_r \times s - \sum_{in} m_r \times s = \sum \frac{Q_{cv}}{T} + \sigma_{cv} \quad (9)$$

The model and method are described in detail, elsewhere, (Nawaz and Ally, 2019); Ally, *et al*., 2015). Suffice to mention that **Eq. (8)** and **Eq. (9)** are applied to each component and to the connecting lines to determine the entropy generation which is subsequently aggregated to yield the total systemic irreversibility. Of the 4 cooling cases in **Table**

4, for brevity we present the results for 35C_H and 35C_L, below. Note that the total irreversibility losses are substantially greater for the high-speed case than for the low-speed case. R-452B and R-454B have the lowest irreversibility.

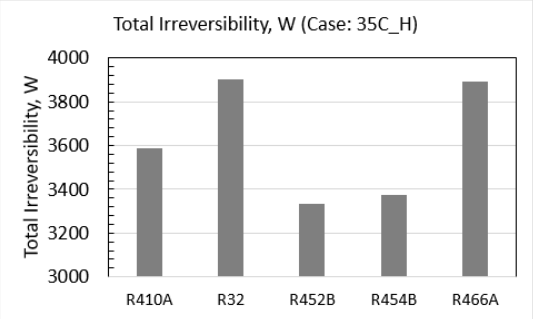

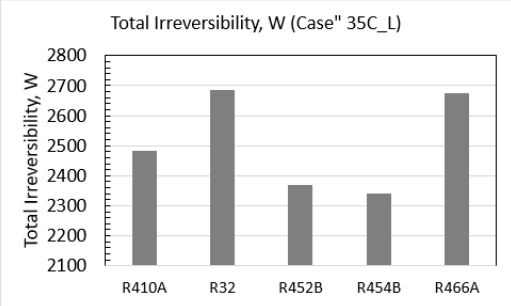

Figure 10: The total systemic irreversibility when the compressor speed is high (left) and low (right).

5. HEATING PERFORMANCE

Table 5 below presents predicted heating performances of the heat pump using R-410A at the low (_L) and high speed (_H) levels, including capacities [kW], COPs [W/W], compressor discharge temperature [C/F] and compressor isentropic defined in the form of **Eq. 2**.

Table 5: Predicted Heating Performance Using R-410A

Outdoor Condition	Capacity [kW]	COP [W/W]	Compressor Disc T [C/F]	Isentropic efficiency
8.3C_H	17.6	3.9	75.05/167.1	72%
1.7C_H	15.0	3.6	74.83166.7	70%
"-8.3C"_H	11.4	3.0	78.22172.8	64%
16.7C_L	15.8	4.5	74.28165.7	66%
8.3C_L	12.8	3.9	74.28165.7	63%
1.7C_L	10.8	3.4	76.72170.1	59%
"-8.3C"_L	7.9	2.6	88.22190.8	50%

Below 15°F, the high-speed operation can't meet the building heating load so supplemental resistance heat must be used. **Figure 11** shows capacity increments of the alterative refrigerants versus R-410A in heating mode. R-32 and R-466A result in 6% to 8% higher heating capacities, which increase with decreasing ambient temperatures. On the other hand, R-452B and R-454B lead to approximately 2% to 6% smaller capacities, which decrease with the ambient temperature. **Figure 12** shows increments in the heat pump heating COPs. R-32 and R-466A lead to 2% lower COPs due to the increased heating capacities. R-452B and R-454B lead to 2% higher COPs. **Figure 13** presents compressor discharge temperatures. Because of the noticeably lower isentropic efficiency of the low speed at low ambient temperatures, more compressor power is converted to heat the refrigerant vapor than providing more useful pressure energy. Thus, the compressor discharge temperatures at low speed are higher than those at high speed. This is opposite to the trend, shown in **Figure 8** regarding the cooling mode.

The discharge temperature increases with the pressure ratio, which tends to be higher in heating mode. Limit of discharge temperature is the major reason preventing heat pump operating below a certain ambient temperature. The higher discharge temperatures of the R-410A replacements would narrow the working envelope. The significantly higher discharge temperatures of R-32 (>98.9°C (210°F) at -8.3°C) would require compressor lubricant change for the heat pump application. **Figure 14** compares the seasonal heating COP, i.e. HSPF calculated by AHRI 210/240. Larger heating capacity causes degradation in heat pump COP, however, it decreases the supplemental resistance heat

use at low ambient temperatures. As a result, the seasonal heating COPs are almost identical, regardless of the variations in heating capacity.

5.1 Exergy Analysis (Heating)

Exergy analysis for the most stringent ambient condition of -8.3C_H and -8.3C_L are summarized in Figure 14. Note that the systemic irreversibility is less for the low speed case than for the high speed case.

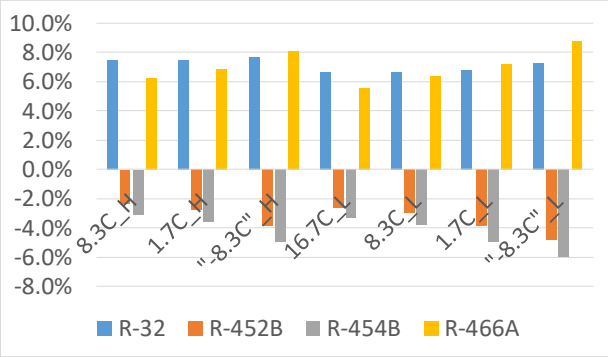

Figure 11: Capacity increments in heating mode

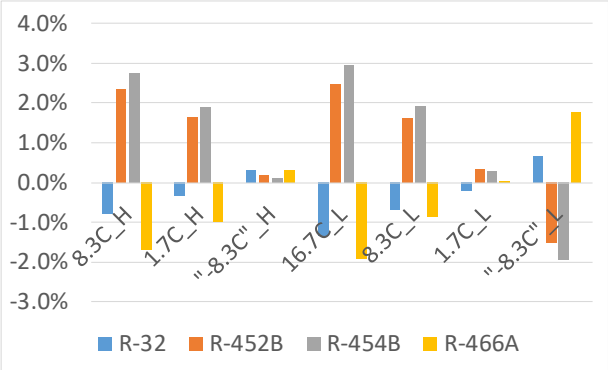

Figure 12: COP increments in heating mode

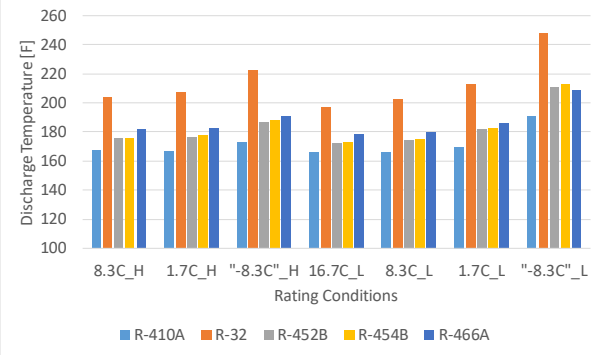

Figure 13: Compressor discharge temperatures in heating mode

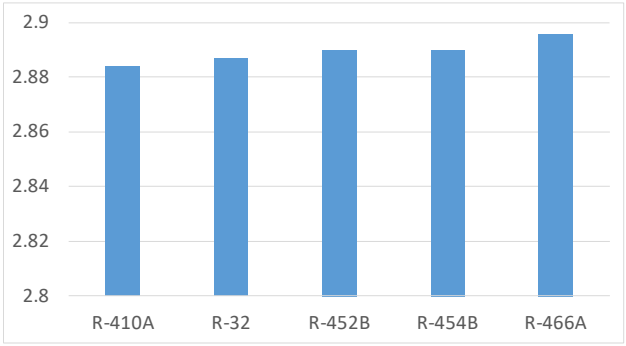

Figure 14: Seasonal heating COPs

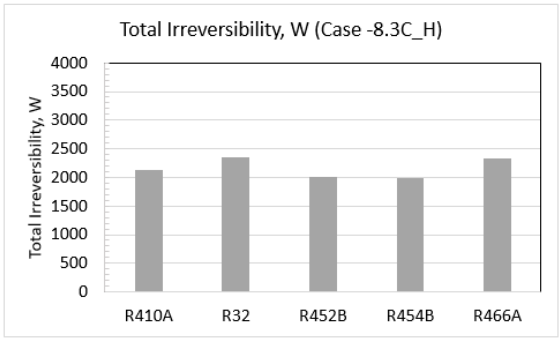

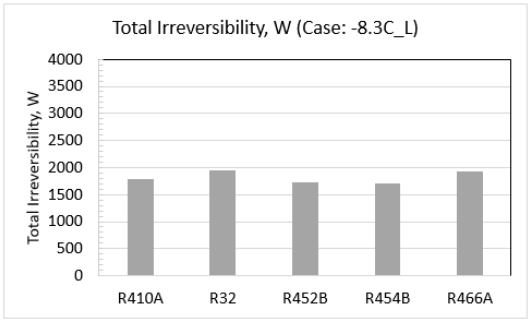

Figure 15: Total systemic irreversibility (heating mode) when the compressor speed is high (left) and low (right).

6. CONCLUSIONS

The low-GWP refrigerants (R32, R454B, R466A, and R452B) are valid replacements for existing R-410A with comparable, and in some cases improved performance metrics.

ACKNOWLEDGEMENT

The authors thank the U.S DOE/Buildings Technology Office and Mr. Anthony Bouza for supporting this work.

NOMENCLATURE

E	total energy	(J)
Q	thermal energy	(W)
W	mechanical work	(W)
h	enthalpy	($J \cdot kg^{-1}$)
s	entropy	($J \cdot kg^{-1} \cdot K^{-1}$)

Subscript

cv	control volume
L	liquid
V	vapor
b	normal boiling point

REFERENCES

Ally, M. R.; Sharma, V.; and Nawaz, K. (2019) "Options for low–global-warming-potential and natural refrigerants Part I: constrains of the shape of the PT and TS saturation phase boundaries." *Int. J. Refrig.*, vol 106, 144-152. https://doi.org/10.1016/j.ijrefrig.2019.05.010

Ally, M. R., Munk, J. D., Baxter, V, D., Gehl, A. C,. 2015. Exergy analysis of a two-stage ground source heat pump with a vertical bore for residential space conditioning under simulated occupancy. *Applied Energy* 155 (2015) 502-514. http://dx.doi.org/10.1016/j.apenergy.2015.06.004

AHRI. (2008). Standard 210/240-2008. "Performance Rating of Unitary Air Conditioning and Air-Source Heat Pump Equipment", Air Conditioning, Heating, and Refrigeration Institute, Arlington, VA.

ANSI/AHRI Standard 540-99. (2010). "Positive Displacement Refrigerant Compressors and Compressor Units", Air Conditioning, Heating, and Refrigeration Institute, Arlington, VA.

Bell, K. J. (1972). An approximate generalized design method for multicomponent/partial condensers. In *AIChE Symp. Ser.* (Vol. 69, pp. 72-79).

Braun. J.E., Klein. S.A, and Mitchell, J.W. (1989). "Effectiveness models for cooling towers and cooling coils", *ASHRAE Trans.*, Vol. 95, Pt. 2, pp. 164-174.

Cavallini, A., Col, D. D., Doretti, L., Matkovic, M., Rossetto, L., Zilio, C., & Censi, G. (2006). Condensation in horizontal smooth tubes: a new heat transfer model for heat exchanger design. *Heat transfer engineering*, *27*(8), 31-38.

Dabiri, A. E., & Rice, C. K. (1981). A compressor simulation model with corrections for the level of suction gas superheat. *Ashrae Transactions*, *87*(Part 2), 771-782.

Kedzierski, M. A. and Choi J. Y. (1999). A generalized pressure drop correlation for evaporation and condensation of alternative refrigerants in smooth and micro-fin tubes, NISTIR 6333.

Morrison, G, 1994. The shape of the temperature-entropy saturation boundary, *Int. J. Refrig*. Vol 17 Number 7, 494-504.

Rouhani, S. Z., & Axelsson, E. (1970). Calculation of void volume fractions in subcooled and quality boiling regimes. *International Journal of Heat and Mass Transfer*, *13*, 383-393.

Shen, B. and Rice, K., 2016, DOE/ORNL Heat Pump Design Model, Web link: http://hpdmflex.ornl.gov/

Shen, B., Abdelaziz, O., Shrestha, S., and Elatar, A. (2018). Model-based optimizations of packaged rooftop air conditioners using low global warming potential refrigerants, *Int. J. of Refrig*., Vol. 87, 106-117.

Stephan, K. (1992). *Heat transfer in condensation and boiling* (p. 84). New York, NY: Springer-Verlag.

Thome J.R. and Jean Ei Hajal. (2002). "Two-phase flow pattern map for evaporation in horizontal tubes: latest version", 1st International Conference on Heat Transfer, Fluid mechanics, and Thermodynamics, 8-10 April 2002, Kruger Park, south Africa TJ2.